Magnetically tuned resonant photon-assisted tunneling

G. S. Vieira,[1,*] J. M. Villas-Bôas,[2] P. S. S. Guimarães,[3] Nelson Studart,[2] J. Kono,[4] S. J. Allen,[4] K. L. Campman,[5] and A. C. Gossard[5]

[1]*Instituto de Estudos Avançados, Centro Técnico Aeroespacial, 12228-840 São José dos Campos, São Paulo, Brazil*
[2]*Departamento de Física, Universidade Federal de São Carlos, 13565-905 São Carlos, São Paulo, Brazil*
[3]*Departamento de Física, Universidade Federal de Minas Gerais, 30123-970 Belo Horizonte, Minas Gerais, Brazil*
[4]*Center for Terahertz Science and Technology, University of California at Santa Barbara, California 93106, USA*
[5]*Materials Department, University of California at Santa Barbara, California 93106, USA*

(Received 31 October 2003; revised manuscript received 5 February 2004; published 26 July 2004)

We present evidence of a new channel for electronic conduction in a multi-quantum well type superlattice in the presence of a magnetic field applied parallel to the quantum well layers. Electrons in one potential well that are photo-excited to anti-crossings of the dispersion curves of the conduction subbands tunnel resonantly to the neighboring wells without intrasubband relaxation. This tunneling mechanism must be distinguished from tunneling involving states located around the energy minimum of the conduction subbands. We show that the new tunneling channel can only be understood from a nonperturbative calculation of the energy levels of the multi-quantum well structure in the presence of the magnetic field, since first order perturbation theory predicts the same energy dispersion for all conduction subbands, thus making this tunneling channel indistinct from standard intersubband excitation. Measurements of THz photocurrent show that both tunneling processes co-exist in a GaAs/AlGaAs multi-quantum well superlattice.

DOI: 10.1103/PhysRevB.70.035316 PACS number(s): 73.21.Cd, 73.40.Gk, 73.63.Hs

I. INTRODUCTION

Photon-assisted tunneling has been extensively studied[1] in multi-quantum well type superlattices (MQW). The strong interest in optical intersubband transitions in such structures is driven not only by its fundamental physics appeal but also by its applications for infrared sources and detectors. Quantum well infrared photodetectors based on intersubband transitions[2] and the quantum cascade laser[3,4] which relies on photon-assisted tunneling between quantized states in a MQW structure, have achieved a high level of performance and are nowadays a commercial reality. When the photon energy does not coincide with any intersubband gap, tunneling through virtual states can be observed. This tunneling through photon side bands, first observed by Tien and Gordon[5] in superconductor-insulator-superconductor systems, has also been widely investigated.[6–8] In a previous paper,[9] we have experimentally explored the connection between the two processes with radiation in the THz range.

The application of a quantizing magnetic field is a powerful tool to study the electron dynamics in quantum well structures. Recently, magnetic fields were used to study the transition to quantum chaos in a semiconductor superlattice.[10] The application of THz radiation in the presence of a tilted magnetic field has been shown to lead to a complex set of phenomena.[11] A magnetic field applied parallel to the MQW layers (perpendicular to the tunneling current) changes the electron states, thus providing an extra degree of freedom to manipulate the electronic band structure and the resonant tunneling conditions. The parallel magnetic field modifies the electron energy dependence on k_y, the wavevector component perpendicular to both the field and growth directions. At the anti-crossings of the k_y dispersion relations the electron wave functions are extended over more than one well and therefore the states at the anti-crossings constitute tunneling channels.[12,13] If the electrons are at thermal equilibrium inside each subband, only those tunneling channels coincident with the bottom of the occupied subbands (or around it) will be observed in transport measurements. In this process, when a higher energy subband is populated by photo-excitation, the photo-excited electrons will first relax energy and decay to the lowest energy states of this subband before tunneling.

In this paper, we propose a distinct resonant photon-assisted tunneling process in which electrons are excited directly into extended states at the anti-crossings in the k_y dispersion relations, away from the bottom of any subband. Hence, a significant fraction of these electrons tunnel to a neighboring well before relaxing energy. We probe this tunneling channel in a GaAs/AlGaAs multi-quantum well superlattice under a parallel magnetic field with photocurrent measurements using THz radiation. Our measurements show evidence for resonant photon-assisted electron tunneling with and without previous relaxation to the bottom of the first excited subband.

The effect of a parallel magnetic field on the electronic states is usually treated according to first order perturbation theory.[14,15] According to perturbation theory, the dispersion relations of different subbands, at zero bias, are equal, if effects due to nonparabolicity of the effective mass are not considered. This means, at least for low biases and large wells, that the resonance frequency for photo-excitation between subbands would not depend strongly on k_y. Hence, first order perturbation theory does not predict a significant difference in the resonance frequency for direct photo-excitation from the first subband into the extended states at the anti-crossings in the k_y dispersion relations of higher subbands, away from their minima, and the resonance frequency for excitation between states at the bottoms of the lowest subband and of an excited one. A numerical nonperturbative

calculation shows that these two frequencies are appreciably different and the former has a stronger dependence on the applied parallel magnetic field, in agreement with the observed photocurrent results. It is important to stress here that the difference in the two frequencies mentioned above will be measurable only for MQW structures with large wells, i.e., for structures in which the lowest energy subbands are close (a few meV) to the bottom of the conduction band, since it is in this case that first order perturbation theory should not be a good approximation even for moderate magnetic fields ($B \sim 5$ T).

II. EXPERIMENTAL SETUP

The sample used in this work was grown by molecular beam epitaxy over a semi-insulating GaAs substrate. It consists of a superlattice made of ten layers of GaAs and eleven layers of $Al_{0.3}Ga_{0.7}As$ sandwiched between two layers of GaAs, each 50 nm thick. All these layers are uniformly doped with Si to 3×10^{15} cm^{-3}. This structure was again sandwiched between two 300 nm thick GaAs layers heavily doped with Si at 2×10^{18} cm^{-3}. The nominal thicknesses of the GaAs wells and $Al_{0.3}Ga_{0.7}As$ barriers are 33 nm and 4 nm, respectively. In a previous work with the same sample,[9] the resonance frequency of the first intersubband transition, at zero magnetic field, was measured as (3.27 ± 0.05) THz. Comparing this value with a simple envelope function calculation for an isolated well, the real width of the wells was assumed to be 31.7 nm.

Very small mesas were fabricated photolithographically for the vertical transport experiments, with an active area of 2×4 μm^2. The mesas were integrated into a bow-tie antenna to achieve better coupling to the THz radiation. The antenna has Ohmic contacts made to the top and bottom heavily doped layers. Since the power coupled to the device is a sensitive function of the frequency, a Schottky diode was integrated into the bow-tie to normalize the power coupled to the superlattice device, as described elsewhere.[9] All experiments presented here were done after adjusting the power of the THz radiation in order to achieve the same photoinduced current in the Schottky diode. This power was chosen low enough to not generate any feature related to photon side bands.

The THz radiation source was a continuously tuning free electron laser (FEL) of the University of California at Santa Barbara. It is a pulsed laser with a repetition rate of 0.75 s and a pulse width around 2 μs. The photocurrent in the superlattice was measured as the difference in current during the FEL pulse and between pulses, using a digital oscilloscope.

To apply the magnetic field, a split coil superconductor magnet with four optical windows was used. The measurements presented in this paper were done at a temperature of (24 ± 3) K and always with the magnetic field applied parallel to the semiconductor layers (perpendicular to the tunneling current).

III. THEORETICAL CONSIDERATIONS

Let $V(z)$ be the MQW potential and consider a magnetic field applied parallel to its layers in the x direction. Using the asymmetric gauge $\vec{A}=(0,-zB,0)$ and the effective mass approximation, the Hamiltonian of an electron in the conduction band can be expressed as

$$H=\frac{p_x^2}{2m^*}+\frac{m^*\omega_c^2}{2}\left(\frac{p_y}{eB}-z\right)^2+\frac{p_z^2}{2m^*}+eV(z), \tag{1}$$

where e is the electron charge, B is the magnetic field intensity, m^* is the effective electron mass, p is the canonical momentum, and $\omega_c=eB/m^*$ is the cyclotron frequency.

We performed a nonperturbative numerical calculation in the effective mass approximation by expanding the Hamiltonian (1) in the basis of an infinite square well much larger than the MQW potential in the z direction, and then we solve the resulting eigenvalue problem for different k_y and B values. We consider different effective masses for the electron in the potential barriers and wells. The size of the basis used was chosen by a test of convergence, which compares the eigenvalues obtained for different sizes of the basis and the convergence is assumed when the difference between them is smaller than 10^{-5}. For the sake of comparison with the exact theoretical results and their interpretation, we also evaluated the energy subbands within perturbation theory. Furthermore, as stated in the Introduction, previous experiments have been analyzed using first-order perturbation theory. In this case, considering the magnetic field contribution as a perturbation, the energy eigenvalues are given by[15]

$$E_n=E_n'+\frac{e^2B^2}{2m^*}\left[(\langle z^2\rangle_n-\langle z\rangle_n^2)+\left(\frac{\hbar k_y}{eB}+\langle z\rangle_n\right)^2\right]+\frac{\hbar^2k_x^2}{2m^*}, \tag{2}$$

where $\langle z\rangle_n$ and $\langle z^2\rangle_n$ are, respectively, the expectation values of z and z^2 for the unperturbed wave functions of subband n and E_n' is its unperturbed energy eigenvalue. The wave function of isolated wells should be used in the calculation of the expectation values, since the solution above does not consider the coupling among wells. One should note that the bottom of each subband will now be at $k_x=0$ and $\hbar k_y/eB=-\langle z\rangle_n$.

Tunneling channels in the MQW are associated to crossings between dispersion curves of subbands localized at different wells. For a sequential tunneling process, as it is the case considered here, only crossings between subbands of adjacent wells need to be considered. A maximum in electron tunneling will occur whenever a crossing between subbands of adjacent wells happens at the bottom of an occupied subband.[14] Therefore, considering a constant electric field, a maximum in the tunneling current is expected at the value of the magnetic field at which there is a crossing between the first subband of one well with the bottom of the first subband of the adjacent well. For this situation, first-order perturbation theory gives the following relation between the voltage drop ΔV per period d of a MQW and the magnetic field position $B_{\max}$ of the maximum in the current:

$$e\Delta V=\frac{e^2d^2}{2m^*}B_{\max}^2. \tag{3}$$

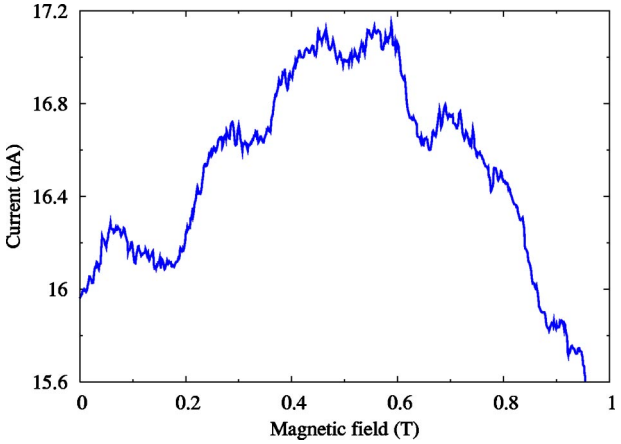

FIG. 1. (Color online) Current as a function of the magnetic field parallel to the MQW layers, measured at a fixed bias of 15 mV without illumination. A broad peak is seen around 0.49 T, the field for the resonance condition shown in Fig. 2. The sharper features are not reproducible and should be understood as noise.

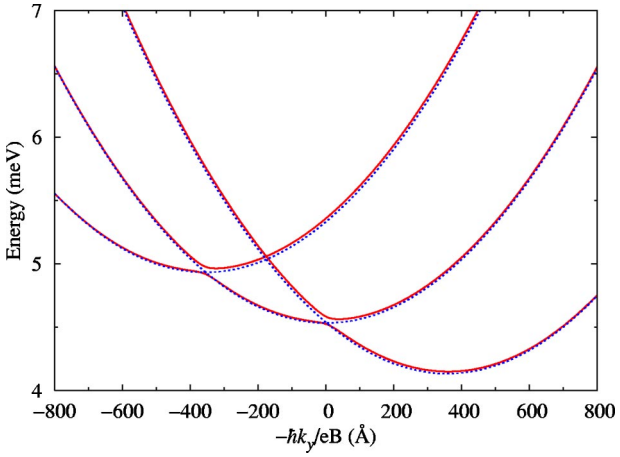

FIG. 2. (Color online) The lowest energy levels of three adjacent potential wells as a function of $-\hbar k_y/eB$, the so-called cyclotron orbit center, at a magnetic field of 0.49 T and a voltage drop of 0.4 mV per period, calculated by the numerical nonperturbative calculation described in the text (solid line) and using first-order perturbation theory (dotted lines). For these values of magnetic and electric fields the first subband of the right well is at resonance with the bottom of the first subband of the center well, near $k_y=0$.

It is clear that first-order perturbation theory fails for large magnetic fields, when the magnetic quantization energy becomes comparable to the separation between the energy levels of the wells. However, it is a good approximation for low enough fields.

IV. RESULTS AND DISCUSSION

We measured the current, I, without illumination, as a function of the parallel magnetic field, B, for a fixed bias of 15 mV across the sample. At this low voltage, since only the first subband of the wells is occupied, electronic conduction occurs via resonant tunneling from the first subband of one well to the first subband of the neighboring well. As shown in Fig. 1, a single broad maximum is observed in the $I-B$ curve at $B_{\max}=(0.49\pm0.05)$ T. From Eq. (3) we obtain a voltage drop per period of (0.40 ± 0.08) mV for the total bias of 15 mV. This means that a relatively large voltage is dropped in the contacts of the structure at this low bias.

Figure 2 shows the lowest energy levels of three adjacent wells as a function of $-\hbar k_y/eB$ for a magnetic field of 0.49 T and a voltage drop per period of 0.4 mV. As expected, for these conditions the first subband of one well is at resonance with the bottom of the first subband of a neighboring well, thus opening up a tunneling channel between these two wells. The energy levels were calculated numerically, as described above, and also by first-order perturbation theory with the sample parameters given in Sec. II. For this low magnetic field, the nonperturbative calculation gives almost the same dispersion curves as perturbation theory, except that the crossings between subbands of different wells become anti-crossings. The use of Eq. (3) at this field is accordingly justified.

Figure 3 shows a comparison of the energy levels of three adjacent wells as a function of $-\hbar k_y/eB$ calculated numerically and by first-order perturbation theory, for a magnetic field of 3.1 T and a voltage drop of 0.4 mV per period of the MQW superlattice. The perturbation theory dispersion relations for the second subband cannot be distinguished from the numerical calculation, but the difference in the first subbands is already clear. Note that this difference increases when k_y moves away from the subband minimum.

The second subbands of the wells in the MQW superlattice can be populated by illumination. If the second subbands are occupied and the sample is under a magnetic field at which there is an anti-crossing at their bottom, electron tunneling will occur to the subband with which the anti-crossing is happening. For a voltage drop per period of 0.4 mV, such a condition will be met at $B=0.49$ T, for tunneling from second to second subbands (the same field position as the resonance from first to first subbands), and for $B=3.1$ T for

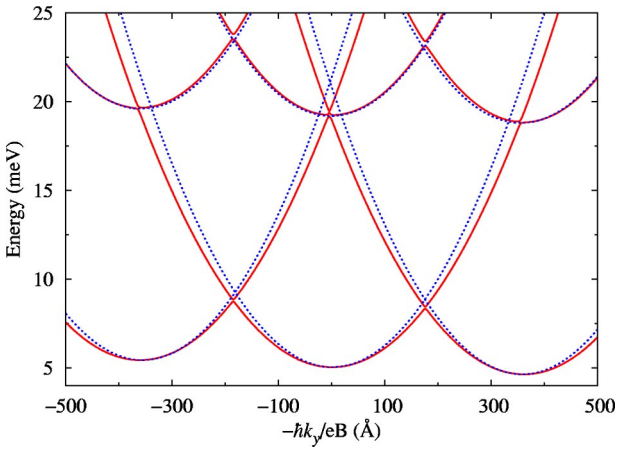

FIG. 3. (Color online) Dispersion relations of a three well structure at $B=3.1$ T and a voltage drop of 0.4 mV per period, calculated using first order perturbation theory (dotted lines) and by the numerical nonperturbative calculation described in the text (solid line). In this case, there are anti-crossings at the bottom of the second subbands with the first subbands of the neighboring wells.

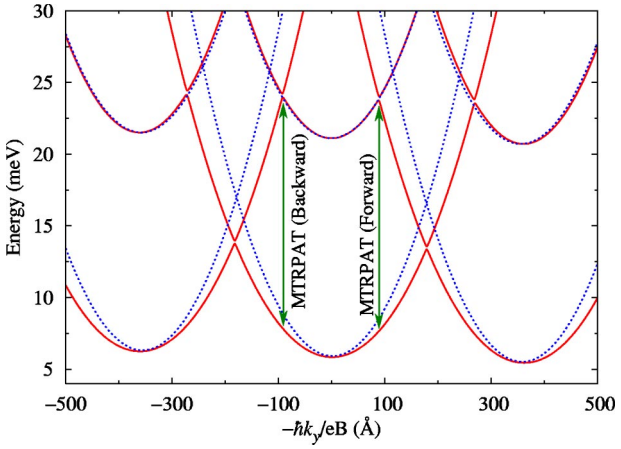

FIG. 4. (Color online) Dispersion relations of a three well structure at $B=5.1$ T and a voltage drop of 0.4 mV per period, calculated using first-order perturbation theory (dotted lines) and by the numerical nonperturbative calculation described in the text (solid line). The arrows show the excitation energy from the first subband of the center well into extended states at the anti-crossings between the second subband of this same well and the first subbands of the neighboring wells.

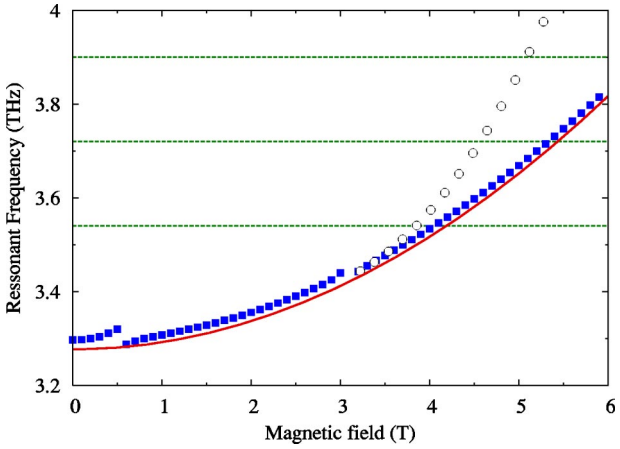

FIG. 5. (Color online) Calculated resonant frequency for the magnetically tuned resonant photon-assisted tunneling, MTRPAT (open circles) and for the excitation between states at the bottom of the lowest subband and of the second one (closed squares). The dependence on the magnetic field of the intersubband excitation frequency given by first-order perturbation theory is also shown (solid line). The horizontal dashed lines show the frequencies used in the measurements. The intersection of them with the MTRPAT curve gives the resonance fields for magnetically tuned resonant photon-assisted tunneling at these frequencies.

tunneling from second to first subbands (Fig. 3). Here perturbation theory gives a result just slightly different, $B=2.9$ T, for the magnetic field at which the latter crossing occurs. If THz radiation is applied to the MQW biased at 0.4 mV per period, at a frequency near the intersubband excitation resonance between first and second subbands, peaks in the photocurrent should be seen at those magnetic fields. It should be remembered that the excitation resonance frequency will also change with B, due to the diamagnetic shift.

The electrons photo-excited by THz radiation to the second subband of the MQW come from states between the bottom of the first subband and the local Fermi level. Here the differences between the nonperturbative calculation and the first-order perturbation theory results become more apparent. According to perturbation theory, the resonance frequency for all these electrons should be almost the same (there is a small difference due to the presence of the electric field). In contrast, as can be seen in Fig. 3, the numerical results give an excitation energy that increases as k_y moves away from the first subband minimum due to the difference in the curvatures of the dispersion curves of the first and the second subbands. This difference in curvature increases as the magnetic field increases, as is demonstrated in Fig. 4. This effect leads to a broadening of the transition frequency as the magnetic field rises. Note that it is an asymmetrical broadening, since it opens the possibility for electrons to be excited by higher radiation frequencies but not by lower frequencies.

The difference in the curvatures of the dispersion curves of the first and the second subbands makes it possible to observe a channel for photon-assisted tunneling at a resonance frequency distinct from the excitation frequency corresponding to the transition between the lowest levels of the first and the second subbands. This new frequency is shown by the arrows in Fig. 4. In this process, electrons from the first subbands are excited directly into extended states at the anti-crossings between the second subband of one well and the first subband of the adjacent wells, but the anti-crossings do not happen at the bottom of the second subband, as it is the case in Fig. 3. The resonant frequency for this magnetically tuned resonant photon-assisted tunneling (MTRPAT) is higher than the frequency for photo-excitation between the lowest levels of the first and the second subbands.

In a measurement of the photocurrent as a function of magnetic field, in the MQW biased at 0.4 mV per period and illuminated with radiation of frequency higher than the frequency for the intersubband resonance at 3.1 T (see Fig. 3), the MTRPAT tunneling channels should show up as an additional peak at a magnetic field higher than 3.1 T. If this maximum in the tunneling current will really show up or not depends on the energy position of the first subband quasi-Fermi level, since the electrons are coming from an excited state of the first subband, as shown in Fig. 4. The peak in the photocurrent at 3.1 T should still be seen at frequencies higher than the corresponding resonant frequency due to the fact that most of the electrons photo-excited to states with k_y values away from the bottom of the second subband will relax to states close to $k_y=0$ and then tunnel to the adjacent wells.

Figure 5 shows the calculated resonant frequency for MTRPAT as a function of the parallel magnetic field. The frequency corresponding to the intersubband transition between the bottoms of the first and second subbands is also shown. First-order perturbation theory gives a very good approximation to the latter but fails to account for the MTRPAT at fields higher than ~ 4 T.

In order to verify the predictions above, we have performed measurements of photocurrent as a function of magnetic field for the GaAs/AlGaAs MQW superlattice at three

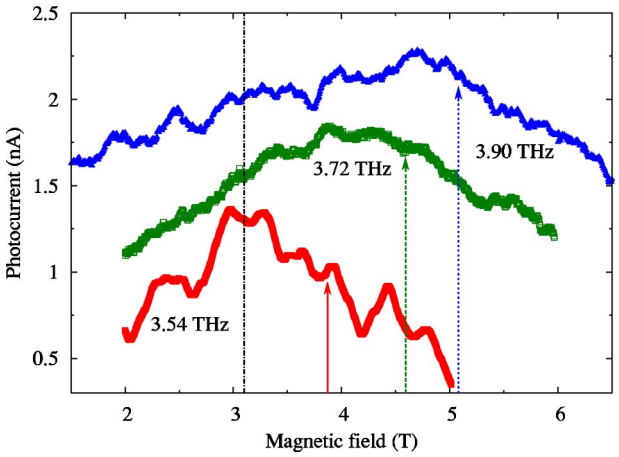

FIG. 6. (Color online) Photocurrent as a function of magnetic field applied parallel to the MQW layers, for three radiation frequencies. The arrows show the expected field positions for MTRPAT at $f=3.54$ THz (solid arrow), at $f=3.72$ THz (dashed arrow) and at $f=3.90$ THz (dotted arrow). The dash-dotted vertical line at 3.1 T shows the field at which another maximum in the photocurrent should occur due to the anti-crossings at the bottom of the second subbands with the first subbands of the neighboring wells. The observed broad (linewidth larger than 1 T) peaks are a result of the convolution of this peak with the MTRPAT resonance, as explained in the text. For the sake of clarity, the curves for $f=3.72$ THz and $f=3.90$ THz were moved up 0.4 and 0.8 nA, respectively.

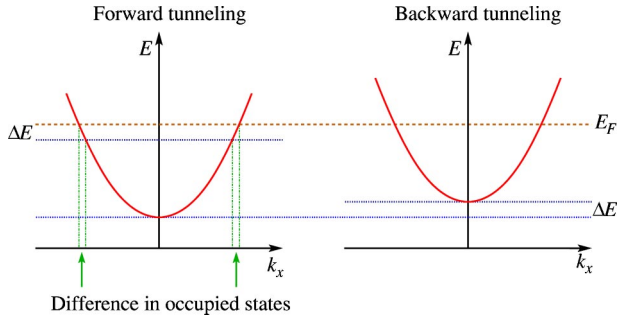

FIG. 7. (Color online) Schematic representation of the k_x dispersion curve for electron states at two different k_y's, at the same subband. It represents states, at the first subband of a well, with k_y's coincident with the edge of the forward and backward MTRPAT channels.

frequencies above the resonance between the bottoms of the two first subbands at $B=3.1$ T. These frequencies (the three horizontal lines in Fig. 5) were chosen because they are outside the water absorption frequency ranges. The results are shown in Fig. 6. There, the expected resonance fields for MTRPAT at the three THz frequencies, taken from Fig. 5, are indicated by the arrows. These fields are $B=3.85$ T for $f=3.54$ THz, $B=4.57$ T for $f=3.72$ THz and $B=5.08$ T for $f=3.90$ THz. Also shown in Fig. 6 is the field (3.1 T) at which another peak in the photocurrent is expected, due to the anti-crossings at the bottom of the second subbands with the first subbands of the neighboring wells. The main broad peaks in the photocurrent, which are clear and reproducible, are the result of the superposition of these two resonances. The sharper features are not reproducible and should be understood as noise. Comparisons of the total photocurrent between curves at different frequencies should consider that there might be a difference in the radiation power coupled to the MQW of the order of 40%, in spite of the adjustment of the current in the Schottky diode integrated into the bow-tie antenna contacts, as described above.

The photocurrent curve for $f=3.90$ THz shows a broad asymmetric maximum near the expected field position for the MTRPAT resonance at this frequency. As the radiation frequency goes down, the resulting maximum narrows and shifts to $B=3.1$ T for $f=3.54$ THz. In accordance with the discussion above, the observed maxima in the photocurrent arise as the result of the superposition of two peaks: one at $B=3.1$ T, where there is a maximum for the tunneling probability for electrons at the bottom of the second subband, and another at the MTRPAT resonance. As f decreases, the two peaks get closer. This leads to a narrowing of the resulting maximum in the photocurrent, in agreement with the results shown in Fig. 6. The data in Fig. 6 also shows that the relative intensity of the two peaks changes with frequency. The relative weight of the peak at $B=3.1$ T increases as the radiation frequency goes down. This is expected, since as the radiation frequency approaches the excitation resonance between the bottoms of the first and the second subbands at $B=3.1$ T, the photon-generated population of the second subbands at this field increases. In addition, the MTRPAT peak should increase with the increase of radiation frequency. As the resonant magnetic field for MTRPAT increases, the photo-excited electrons come from states higher in energy in the first subbands. Therefore, as the radiation frequency increases the total number of photo-excited electrons decreases as the energies of the initial states approach the quasi-Fermi levels of the first subbands. The photocurrent is given by the difference between the electrons going through the forward tunneling channels and through the backward tunneling channels (see Fig. 4). It is important to note that the electrons going via the forward tunneling channel are coming from states at the first subbands slightly lower in energy than the electrons going through the backward tunneling channel, due to the applied electric field. This difference, ΔE, is increasing as B increases (it is 0.12 meV for $B=3.86$ T and 0.19 meV for $B=5.10$ T), which leads to an increase of the MTRPAT photocurrent. Furthermore, when the k_x dispersion is considered, the difference in energy between states with the k_y of the forward tunneling channel and with the k_y of the backward tunneling channel also give rise to a difference in the number of initial states for the MTRPAT. Figure 7 shows the k_x dispersion curves at the two k_y's just at the edge of the forward and backward tunneling channels. The two dispersion curves are equal, just vertically shifted by ΔE. At $T=0$ K, considering ΔE constant (even though it actually increases with the magnetic field), the difference in the available electrons for forward and backward MTRPAT increases as the bottom of the two k_x dispersion curves approaches the local Fermi level. Naturally, when the bottom of the higher k_x dispersion curve, the one for backward tunneling, reaches the quasi-Fermi level, the difference between the number of forward and backward MTRPAT

electrons starts to decrease and goes to zero when the bottom of the k_x dispersion curve of forward tunneling gets to the quasi-Fermi level. Consequently, the MTRPAT photocurrent peak should increase with the radiation frequency until near the cutoff frequency.

It is also interesting to note that the photocurrent peak due to MTRPAT should be sharper as the resonant THz radiation frequency increases. This is due to the increasing derivative of the MTRPAT resonance frequency dependence on magnetic field as can be seen in Fig. 5.

V. CONCLUSION

We have predicted and observed a magnetically tuned resonant photon-assisted tunneling process in multi-quantum well superlattices in which electrons are photo-excited directly into extended states at the anti-crossings in the k_y dispersion relations, away from the bottom of the conduction subbands. This tunneling channel is understood with a basis on a nonperturbative numerical calculation of the dispersion curves of the energy subbands in the presence of a magnetic field applied parallel to the quantum well layers. We have investigated this process in a GaAs/AlGaAs superlattice with photocurrent measurements using THz radiation under a quantizing magnetic field. A significant fraction of the electrons, photo-excited to the anti-crossings, tunnel to the neighboring wells of the superlattice before relaxing energy. We have also observed photon-assisted tunneling involving states located around the energy minimum of the conduction subbands. Both photon-assisted tunneling channels co-exist in the experimental conditions used.

ACKNOWLEDGMENTS

The authors thank the whole staff of the UCSB Center for Terahertz Science and Technology for their outstanding support, commitment and expertise. We thank Marcus Antônio Ruggieri Franco and Valdir Augusto Serrão for their help with the initial calculations. The authors also acknowledge the financial support of Conselho Nacional de Desenvolvimento Científico e Tecnológico—CNPq. P. S. S. Guimarães acknowledges the financial support of Fundação de Amparo à Pesquisa de Minas Gerais—FAPEMIG and Instituto de Nanociências. J. M. Villas-Bôas and N. Studart acknowledge the financial support of Fundação de Amparo à Pesquisa do Estado de São Paulo—FAPESP. Research at UCSB was supported by the ONR and the AFOSR.

*Electronic address: gvieira@ieav.cta.br

[1] K. Unterrainer, Semicond. Semimetals **66**, 127 (2000).
[2] A. Rogalski, J. Appl. Phys. **93**, 4355 (2003).
[3] C. Gmachl, F. Capasso, D. L. Sivco, and A. Y. Cho, Rep. Prog. Phys. **64**, 1533 (2001).
[4] H. Willenberg, G. H. Döhler, and J. Faist, Phys. Rev. B **67**, 085315 (2003).
[5] P. K. Tien and J. P. Gordon, Phys. Rev. **129**, 647 (1963).
[6] P. S. S. Guimarães, B. J. Keay, J. P. Kaminski, S. J. Allen, Jr., P. F. Hopkins, A. C. Gossard, L. T. Florez, and J. P. Harbison, Phys. Rev. Lett. **70**, 3792 (1993).
[7] S. Zeuner, B. J. Keay, S. J. Allen, K. D. Maranowski, A. C. Gossard, U. Bhattacharya, and M. J. W. Rodwell, Phys. Rev. B **53**, R1717 (1996).
[8] K. Unterrainer, B. J. Keay, M. C. Wanke, S. J. Allen, D. Leonard, G. Medeiros-Ribeiro, U. Bhattacharya, and M. J. W. Rodwell, Phys. Rev. Lett. **76**, 2973 (1996).
[9] G. S. Vieira, S. J. Allen, Jr., P. S. S. Guimarães, K. L. Campman, and A. C. Gossard, Phys. Rev. B **58**, 7136 (1998).
[10] T. M. Fromhold, A. A. Krokhin, C. R. Tench, S. Bujkiewicz, P. B. Wilkinson, F. W. Sheard, and L. Eaves, Phys. Rev. Lett. **87**, 046803 (2001).
[11] J. M. Villas-Bôas, W. Zhang, S. E. Ulloa, P. H. Rivera, and N. Studart, Phys. Rev. B **66**, 085325 (2002).
[12] G. Platero, L. Brey, and C. Tejedor, Phys. Rev. B **40**, 8548 (1989).
[13] T. M. Fromhold, F. W. Sheard, and G. A. Toombs, Surf. Sci. **228**, 437 (1990).
[14] W. Müller, H. T. Grahn, K. von Klitzing, and K. Ploog, Phys. Rev. B **48**, 11 176 (1993).
[15] J. K. Maan, Festkoerperprobleme **27**, 137 (1987).